Dätwyler Christoph (Orcid ID: 0000-0002-9923-4311)

ENSO variability, teleconnection changes and responses to large volcanic eruptions since AD 1000

Running head: ENSO variability, teleconnections and volcanic eruptions since AD 1000

Christoph Dätwyler, Nerilie J. Abram, Martin Grosjean, Eugene R. Wahl and Raphael Neukom

[1] Institute of Geography and Oeschger Centre for Climate Change Research, University of Bern, 3012 Bern, Switzerland

[2] Research School of Earth Sciences and ARC Centre of Excellence for Climate Extremes, Australian National University, Canberra, Australia

[3] NOAA's National Centers for Environmental Information, Center for Weather and Climate, 325 Broadway Street, Boulder, Colorado (80305), USA

Corresponding author:

Christoph Dätwyler

Erlachstrasse 9a, Trakt 3

3012 Bern

Switzerland

E-mail: christoph.daetwyler@giub.unibe.ch

Phone: 0041 31 631 50 91

This is the author manuscript accepted for publication and has undergone full peer review but has not been through the copyediting, typesetting, pagination and proofreading process, which may lead to differences between this version and the Version of Record. Please cite this article as doi: 10.1002/joc.5983

Key words: climate change, volcanic forcing, natural climate variability, Holocene, paleoclimatology, climate reconstruction, PCA, proxy records

Abstract

The El Niño-Southern Oscillation (ENSO) is the Earth's dominant mode of interannual climate variability. It alternates between warm (El Niño) and cold (La Niña) states, with global impacts on climate and society. This study provides new ENSO reconstructions based on a large, updated collection of proxy records. We use a novel reconstruction approach that employs running principal components, which allows us to take covariance changes between proxy records into account and thereby identify periods of likely teleconnection changes. Using different implementations of the principal component analysis enables us to identify periods within the last millennium when quantifications of ENSO are most robust. These periods range from 1580 to the end of the 17th century and from 1825 to present. We incorporate an assessment of consistency among our new and existing ENSO reconstructions leading to five short phases of low agreement among the reconstructions between 1700-1786. We find a consistent spatial pattern of proxy covariance during these four phases, differing from the structure seen over the instrumental period. This pattern points towards changes in teleconnections in the west Pacific/Australasian region, compared to the present state. Using our new reconstructions, we find a significant response of ENSO towards more La Niña-like conditions 3-5 years after major volcanic events. We further show that our new reconstructions and existing reconstructions largely agree on the state of ENSO during volcanic eruptions in the years 1695 and 1784, which helps put into perspective the climatic response to these events. During all other large volcanic eruptions of the last 1000 years, there is no reconstruction coherency with regards to the state of ENSO.

1 Introduction

The El Niño-Southern Oscillation (ENSO) is one of the most important modes of climate variability (McPhaden, Zebiak, & Glantz, 2006). ENSO variability originates in the equatorial Pacific region (McPhaden et al., 2006; Neelin et al., 1998) and has global impacts on climate and society (Bradley, Diaz, Kiladis, & Eischeid, 1987; Brönnimann, 2007; Yeh et al., 2018 and references therein). ENSO involves a coupled phenomenon between atmospheric and oceanic processes (Neelin et al., 1998) alternating on 2-7 year periods between warm El Niño and cold La Niña states (McPhaden et al., 2006). Long-term knowledge of ENSO is crucial to assess potential teleconnection changes in relation to increased anthropogenic forcing (Yeh et al., 2018) and to quantify relationships between the state of ENSO and the climatic response to volcanic events (Iles & Hegerl, 2015; Lehner, Schurer, Hegerl, Deser, & Frölicher, 2016).

Many ENSO reconstructions covering the last centuries exist already (Braganza, Gergis, Power, Risbey, & Fowler, 2009; Cook, D'Arrigo, & Anchukaitis, 2008; D'Arrigo, Cook, Wilson, Allan, & Mann, 2005; Emile-Geay, Cobb, Mann, & Wittenberg, 2013; Gergis & Fowler, 2009; Li et al., 2011; Li et al., 2013; Mann et al., 2009; McGregor, Timmermann, & Timm, 2010; Stahle et al., 1998; Wilson et al., 2010; Yan et al., 2011). Comparison of these reconstructions reveals substantial differences over the pre-instrumental period (Emile-Geay et al., 2013; McGregor et al., 2010; McGregor, Timmermann, England, Elison Timm, & Wittenberg, 2013). These disagreements strongly hamper analyses and data-model comparisons of ENSO variability over the past centuries. Possible causes for the disagreements between reconstructions include the use of different proxy archives and proxy records with varying spatial coverage, the use of different reconstruction targets and seasons, as well as local noise and uncertainties in the proxy records. Changing teleconnection patterns influencing

remote proxy records may also explain some of the differences seen in ENSO reconstructions (e.g., Batehup, McGregor, & Gallant, 2015; van Oldenborgh & Burgers, 2005; Wilson et al., 2010; cf. Wahl, Diaz, Smerdon, & Ammann, 2014). A systematic assessment of the temporal agreement of existing ENSO reconstructions is important, but currently missing. Consequently, relatively little is known about the causes for the discrepancies among ENSO reconstructions.

The state of ENSO is thought to strongly influence the global climatic response to volcanic eruptions (Iles & Hegerl, 2015; Lehner et al., 2016; cf. Wahl et al., 2014). Knowledge of the state of ENSO at the time of eruptions during the past 1000 years is therefore important for data-model comparisons, in order to assess the capability of models to adequately simulate the climatic response to volcanic forcing. It is also required to correctly interpret the regional to global cooling caused by past eruptions, and to potentially explain weak or lacking signals in large-scale temperature reconstructions for some events (Neukom et al., 2014; PAGES 2k-PMIP3 group, 2015; Raible et al., 2016; Wahl et al., 2014).

ENSO itself may also be influenced by volcanic eruptions (Adams, Mann, & Ammann, 2003; D'Arrigo, Wilson, & Tudhope, 2009; Emile-Geay, Seager, Cane, Cook, & Haug, 2008; Li et al., 2013; Liu et al., 2018; McGregor & Timmermann, 2010; Wahl et al., 2014). Previous ENSO reconstructions suggest an El Niño-like response in the year following an eruption (Adams et al., 2003; Li et al., 2013; Wilson et al., 2010; cf. Wahl et al., 2014 where this response is present in a more muted way). Liu et al. (2018) found a La-Niña like response when only including Southern Hemisphere (SH) eruptions. Other studies found La-Niña-like response in the year of the eruption (Li et al., 2013) and/or three to seven years after the event (Wahl et al., 2014; Wilson et al., 2010). Evaluating climate models, Emile-Geay et al. (2008) found that only eruptions larger than that of the 1991 Mt. Pinatubo eruption have

enough impact to significantly increase chances of an El Niño event following the eruption (cf. Wahl et al., 2014). However, climate models still struggle to correctly represent the responses seen in proxy-based ENSO reconstructions and offer different explanations for the underlying mechanism (Liu et al., 2018; McGregor & Timmermann, 2010; Ohba, Shiogama, Yokohata, & Watanabe, 2013; Stevenson, Fasullo, Otto-Bliesner, Tomas, & Gao, 2017).

Further insight is needed into how ENSO and volcanic eruptions are co-related. The debate concerning how ENSO responds to volcanic events cannot be resolved by recourse to instrumental data due to the lack of large eruptions in the 20th century, and is then amplified by the inconsistent evidence in existing reconstructions. Systematic assessment of the differences seen in existing reconstructions, and the sources of these differences (e.g., changing teleconnections), would lead to improved understanding of the interaction of ENSO variability with volcanic eruptions.

In this study, we first evaluate the consistency of ENSO reconstructions during the last millennium and then assess the effect that teleconnection patterns and proxy network have on ENSO reconstructions. We apply a simple but efficient method based on Principal Component Analysis (PCA) to quantify ENSO and the changing importance of input proxy data over time. This approach and a new large collection of paleoclimate observations allows us to identify periods within the last millennium when quantifications of ENSO are most robust, and also to detect less robust intervals when teleconnection patterns may have changed. We then incorporate an assessment of consistency among our new and existing ENSO reconstructions to more rigorously assess the role of large volcanic eruptions on ENSO during the years following these events.

2 Data and Methods

2.1 Data

Our reconstruction target is the NINO3.4 index, defined as the area average sea surface temperature (SST) anomaly from 5°N-5°S and 170°-120°W (Barnston, Chelliah, & Goldenberg, 1997). We calculate the NINO3.4 index using the ERSSTv5 (Extended Reconstructed Sea Surface Temperature, Version 5) instrumental data set (Huang et al., 2017). The monthly data values were annualised by calculating calendar year (January to December), equally-weighted averages.

Our proxy dataset is a large collection of records combined from different data sources. They consist of the new PAGES 2k global temperature database (Data Citation 1), a collection of SH proxy records including non-temperature sensitive records (Data Citation 2), a recent collection of Antarctic ice core isotope records (Data Citation 3), and additional hydroclimate records from the Northern Hemisphere (NH) that were used in recent ENSO reconstructions (Data Citation 4; Data Citation 5). Most of the proxy records in these data sources are annually resolved. Where records have sub-annual resolution (corals), we use an April-March average to generate annual resolution data (Tierney et al., 2015), which reflects the "tropical year" and does not interrupt the most important growing/response seasons in the SH and the tropics (in contrast to a calendar year window). This annual window also accounts for the lagged response time of temperature and hydroclimate to ENSO (which is averaged herein over calendar years), typically spanning a few months (Su, Neelin, & Meyerson, 2005). In addition, using the calendar year average for the target ENSO index, in contrast to April-March means, yields higher performance values in our reconstructions, and averaging over 12 months takes the strong seasonally varying response of proxy records into account.

To be able to quantify ENSO changes over the last centuries, we select only proxy records that are significantly related to our target ENSO index at a statistical level of $p < 0.05$, taking lag-one autocorrelation into account (Santer et al., 2000). This analysis is carried out over the reference

period 1930-1990, which reflects a compromise between having as many years as possible and excluding periods when the coverage of instrumental data (at the beginning of the period) and proxy data (towards present) is sparse.

Of the whole proxy record collection (743 proxy records), we first select only those 726 proxy records (Figure 1, red and black dots together) with a data gap no longer than 30 years in the period 1930-1990. 81 records significantly correlate ($p < 0.05$) with ENSO over the 1930-1990 reference period (red dots in Figure 1). Missing values (1.8%) in the reference period were infilled using the Composite-Plus-Scale (CPS) method (Neukom et al., 2014), which estimates the missing values of each proxy by a correlation-based weighted average of all other proxies. The selected proxy records are distributed globally, with clusters in the Australasian region and the western North and South American coastline, i.e. around the Pacific domain. Further details about the proxy data can be found in the supplementary material (SM) Table S1.

2.2 Methods

Because the number of proxy records decreases back in time, we perform our analyses over five different subsets of the proxy database covering different temporal windows: 1000-1990, 1400-1990, 1600-1990, 1800-1990 and 1854-1990. Henceforth we call them the 1000 subset, 1400 subset, 1600 subset, 1800 subset and 1854 subset, respectively. For each of these subsets we select those proxy records covering the respective time period. We allow for no more than 20% of missing values in each proxy record over the respective period and replace missing values with the CPS method. This yields a collection of 8 records for the 1000 subset, 18 for the 1400 subset, 32 for the 1600 subset, 51 for the 1800 subset and 60 for the 1854 subset. The distribution of the proxy records on the world map for the respective subsets is shown in Figures S1-S5 in the SM.

Instead of choosing a classical calibration approach to quantify ENSO based on our proxy data collection, we use the first principal component (PC1) of all proxy records that were selected as described above (e.g., Braganza et al., 2009; McGregor et al., 2010). In a spatially well-distributed proxy collection, the first few leading principal components (PCs) will contain information that is coherent across the whole set of proxy records, whereas non-coherent factors such as local climate effects, proxy archive-specific noise (e.g., caused by biological factors), or noise unrelated to climate will be represented by higher order PCs (Braganza et al., 2009). Given the strong influence of ENSO on interannual climate variability over much of the globe and because we have selected the records based on their correlation with the ENSO index, we expect a strong ENSO signal in the first PC of the selected proxies (Braganza et al., 2009). This simple approach to extract the ENSO signal from the proxy data has a key advantage over the calibration approaches typically used in climate reconstructions: it is independent from the target dataset and instead relies on the common signal among a set of records that all demonstrate a significant relationship to ENSO in the instrumental period. This means that the PCs can be calculated over any time period and are not restricted to the overlap period with instrumental data. Details on how we make use of this PCA approach to quantify ENSO back in time are provided in the following section.

2.2.1 Reconstructions

We use three different PCA-based approaches to reconstruct ENSO over the past millennium. For the first approach, we apply a running PCA over the entire reconstruction period. The key strength of this approach is that it overcomes one of the main caveats of calibration-based reconstructions: it is not bound by the assumption that the relationship between the proxies and the target variable is constant over time. The strength of each proxy record's contribution to PC1 (the loadings) may

change over time. If this is the case, the reconstruction based on running PC1 may be different from a reconstruction based on classical calibration. If the loadings show a distinct spatial pattern, then temporal changes in loading patterns may reveal changing teleconnections. Alternatively, changes in individual records that are caused by local climate or non-climatic factors may also lead to temporal variations in the loading factors, particularly if the number of records is low.

The running PCA approach for reconstructing ENSO requires that PC1 continuously shares a large fraction of variance with the ENSO index. To meet this requirement, our proxy network needs to fulfil two conditions: First, the records need to lie within the domain where ENSO influences local climate. Second, the records need to be sufficiently well distributed in space, such that the regional signal from one part of the domain does not explain more common variance in the dataset than ENSO itself. We assume that these criteria are fulfilled if PC1 skilfully captures ENSO variability, which is tested using verification statistics as described below.

We calculate the running PC1 reconstruction as follows: The running PCA is carried out using an 80-year window, with linearly detrended and standardised proxy records over the 80-year intervals. The resulting reconstruction is not sensitive to the choice of the window width. Sensitivity tests with 60- and 100-year windows yield reconstructions that correlate with the 80-year window values at $r = 0.98$ and $r = 0.96$, respectively. The running PCA approach has the consequence that fluctuations at time scales longer than 80 years are not captured by our reconstructions, meaning that we reconstruct ENSO variability up to multi-decadal time scales, but not longer, centennial scale trends. The window of the analysis is shifted backwards by one year starting with 1911-1990 until the earliest 80-year period covered by each proxy subset is reached. We use the prcomp() function in R to calculate the PCA (Becker, Chambers, & Wilks, 1988; Mardia, Kent, & Bibby, 1979; Venables &

Ripley, 2002). For each year, we obtain the running PC1 series by taking the mean of all overlapping standardised 80-year PC1 time series. Note that by taking means the variance in the reconstructed PC1 time series is reduced, especially in the case of fewer and noisy proxy records (similar to classical regression where variance is diminished with more noise in the predictors). Depending on the subset, we call the resulting time series *Running PC1 1000, 1400, 1600, 1800* or *1854*.

The signs of the loadings and PCs are produced randomly by the prcomp() function. Therefore, the signs may need to be reversed before generating the mean running PC1 time series to ensure consistency with the signs of neighbouring time windows. This sign correction was achieved by ensuring that each PC1 slice has a positive correlation during the periods of overlap with the means of the more recent running PC1 slices. That is, going from present to past, if the correlation between the overlap of PC1 of the first and second time window is negative, the second PC1 time window and the corresponding loadings are multiplied by minus one. Then, the mean of those two PC1 time windows is taken and the correlation with the PC1 of the third time window over the overlapping time period is calculated. If negative the third PC1 time series and corresponding loadings are multiplied by minus one. Again the mean over the overlapping period of this third PC1 time series with the previous two PC1 time series is taken, and so forth. This procedure is continued until the last PC1 time window is processed resulting in a suite of sliding 80-year PC1 time series and proxy loadings of consistent sign.

The second approach mimics a classical calibration procedure where the proxy PC1 is calculated only over the reference period when an overlap with instrumental data exists. The proxy records are standardised over the full reconstruction period of each subset prior to calculating the PCA. The

resultant loadings of the proxies on PC1 over the reference period are then multiplied with the complete time series of the proxy records to get a "classic" reconstruction of the PC1.

For consistency with the running PC1 approach, we remove low-frequency fluctuations in the second-approach reconstructions by subtracting an 80-year high pass Butterworth filtered time series from each reconstruction. This process removes longer than 80-year trends but retains interannual variability and is henceforth referred to as 80-year trend removal. Depending on the subset, we call the resulting time series *Overlap Period PC1 1000, 1400, 1600, 1800* or *1854*.

For the third approach, we run a PCA over the entire time period covered by each subset. This approach mimics the hypothetical situation in which the full reconstruction period can be used for calibration. Comparison of the results with the *Overlap Period PC1* allows testing the sensitivity of the reconstructions to the choice and length of the calibration period. The PCA uses standardised proxy records with 80-year trends removed as described for the second approach. Depending on the subset, we call the resulting PC1 time series *Full Period PC1 1000, 1400, 1600, 1800* or *1854*.

Hence, we obtain three different ENSO reconstructions for each subset. Our final three ENSO reconstructions, referred to as *Running PC1*, *Overlap Period PC1* and *Full Period PC1*, are obtained by patching together all five reconstructions in respective temporal order: such that for each year we use the data of the most replicated available subset. Thus, data from the 1000-1990 subset are used for 1000-1399; data from the 1400-1990 subset are used for 1400-1599; data from the 1600-1990 subset are used for 1600-1799; data from the 1800-1990 subset are used for 1800-1853; and data from the 1854-1990 subset are used for 1854-1990. In order to account for changes in variance, the reconstructions are scaled to the variance between 1930-1990 of the target ENSO index over 1000-1399 (for reconstructions based on the 1000 subset), 1400-1599 (for reconstructions based on the

1400 subset), 1600-1799 (for reconstructions based on the 1600 subset), 1800-1853 (for reconstructions based on the 1800 subset) and 1854-1990 (for reconstructions based on the 1854 subset) before patching together to make full-length time series.

To estimate reconstruction uncertainty, an approximation of the 95% confidence range is calculated. Two augmented standard deviations ($SD_{res.aug}$) of the residuals between a reconstruction and the target ENSO index over the reference period 1930-1990 (SD_{res}) are added and subtracted to the respective reconstruction. The formula is as follows:

$$SD_{res.aug} = \sqrt{SD_{res}{}^2 * \left(1 + \frac{1}{n}\right)}$$

The augmentation is derived from the classical formula for the standard error of prediction of an individual fitted value in regression. It results in slightly wider confidence ranges by a factor related to the inverse of the sample size (n), in effect non-linearly penalising smaller samples relative to large ones ("Standard Error of Prediction and Confidence Limits," 2018).

The three approaches we use to reconstruct ENSO variability over the past millennium capture fundamentally different temporal aspects. Applying the running PCA provides the opportunity to detect and quantify the (possibly) changing importance of proxy records to the shared signal over time, contrasting the other two methods where such temporal changes are assumed to be insignificant. Either, they get averaged out by computing PCs over the entire respective subsets or the reconstruction uses only the information of the proxy-ENSO relationship over the reference period. Hence, possible differences in the *Overlap Period PC1* reconstruction in comparison to the *Full Period PC1* reconstruction would imply that the proxy records with the highest loadings on PC1 over the reference period have a smaller contribution to PC1 over the entire subset and vice versa.

The *Running PC1* approach allows us to assess these changes in the importance of proxy records over time by analysing the time series of the loadings of the individual proxy records.

We therefore consider the *Running PC1* as our main reconstruction. It dynamically captures changes in the PC1 and its loadings over time, which might be caused by changing teleconnection patterns.

2.2.2 Validation

All three reconstruction approaches are based on the assumption that the proxy PC1 represents ENSO throughout the last millennium. The capability of the temporal proxy subsets to represent ENSO is assessed by comparing the reconstruction and target ENSO time series over the instrumental reference period (1930-1990). We test this for all subsets. For example, PC1 of the proxy records available in the 1000 subset is compared to the ENSO index over 1930-1990 to estimate the performance of our reconstruction for the period 1000-1399. We proceed accordingly for the other subsets.

To quantify reconstruction skill, we use standard validation metrics over the overlap period of proxy data with the instrumental target ENSO index. They involve reduction of error (RE), r^2 and coefficient of efficiency (CE) (Cook, Briffa, & Jones, 1994). Although we do not perform a calibration of the proxy data with the target, we also calculate validation statistics over 1901-1929, a period independent from the 1930-1990 reference period that was used to select the proxy records.

2.2.3 Loadings on PC1

For each time step in the running PCA, the resultant loadings reflect the importance of each proxy record to the common signal at that specific 80-year long time interval. The greater the absolute value of the loading of a specific proxy record on the first PC1, the stronger its influence in the

reconstruction. The loadings over each 80-year period are assigned to the year in the middle of this 80-year window. Hence, we are able to compare the influence of the proxy records at any point, or over any period in time, by calculating the mean of the loadings corresponding to the respective years in the desired time period. Since we base our analysis on the assumption that PC1 continuously reflects ENSO, a higher loading of a specific proxy record is interpreted as a stronger relation of that proxy to ENSO over the given time period. To facilitate comparison of the spatial loading patterns over any period to the most recent state, we adjust the sign of each proxy record's time series of loadings to be positive over the most recent time interval. On a world map, we show positive loadings in red, negative loadings in blue. Hence, when plotting the loadings over a specific time period, any blue coloured proxy record has changed the sign of its loading on PC1 compared to its most recent state.

2.2.4 Comparison with existing ENSO reconstructions

There are a multitude of existing ENSO reconstructions. They differ in length, target index (e.g. NINO3, NINO3.4, NINO4 or SOI), target season, proxy record selection and reconstruction method. For the analysis of existing ENSO reconstructions and for comparison with our new reconstructions, we consider the reconstructions of Braganza et al. (2009); Cook et al. (2008); D'Arrigo et al. (2005); Emile-Geay et al. (2013); Li et al. (2013); McGregor et al. (2010); Stahle et al. (1998) and Wilson et al. (2010). Other datasets, such as the reconstructions of Mann et al. (2009) and Yan et al. (2011) are not used, since they are not annually resolved and the Yan et al. (2011) reconstruction ends in 1955. In their work, Braganza et al. (2009), Cook et al. (2008) and Emile-Geay et al. (2013) each present more than one ENSO reconstruction, which are highly correlated. For this reason we only use one time series from each: the longest from Braganza et al. (2009), NINO3.4 from Cook et al. (2008), and

the reconstruction based on the ERSSTv3 instrumental target from Emile-Geay et al. (2013). From Wilson et al. (2010), we use both reconstructions (COA and TEL), resulting in a comparison dataset of nine previous ENSO reconstructions.

Paired 11-year running correlations are used to temporally investigate phases of agreement or disagreement among different ENSO reconstructions. An 11-year period was chosen since longer window widths can mask important features of a relatively high frequency phenomenon such as ENSO. The overall agreement is summarised by averaging these running correlations. First, this is done for the nine existing reconstructions. Second, we calculate the mean correlation between our three new reconstructions. Third, to compare our new results with the existing ENSO reconstructions, we calculate running correlations between the *Running PC1* reconstruction and each existing reconstruction and then take the mean of these running correlation time series.

Next, we identify periods of low coherence among ENSO reconstructions. To assess the influence of varying input data and reconstruction methodologies, we use the average running correlations among the existing reconstructions. To test the influence of temporal changes in proxy-covariance, we use the mean running correlation among our three new ENSO reconstructions (*Running PC1*, *Overlap Period PC1* and *Full Period PC1*). We then also identify periods of simultaneous low agreement across these two averaged running correlations. For each averaged running correlation time series, the first quartile is calculated. If both averaged running correlation time series drop below their respective first quartiles simultaneously for at least four consecutive years, we consider this a period of low agreement among all (existing and new) ENSO reconstructions. For the identified periods we compare the corresponding spatial pattern of loadings on PC1 from our new reconstructions, to investigate if a consistent pattern indicative of changing teleconnection patterns

can be observed. Note that the years of the identified periods correspond to the 11-year intervals centred at these dates.

For reference, plots with 31-year running correlations are included in the SM Figure S9. The main spatial pattern of loadings on PC1, corresponding to periods of simultaneous low coherence, remains the same when using 31-year running correlations as when using 11-year running periods, and hence does not depend upon the choice of the window width (SM Figure S10). In addition, the results are robust to alternative methods to define phases of low agreement (SM Section 4.1, Figures S11-S14).

2.2.5 Response to volcanic forcing

The response of our *Running PC1* reconstruction to volcanic forcing is assessed by applying a superposed epoch analysis (SEA, Bradley et al., 1987; Haurwitz & Brier, 1981; McGraw, Barnes, & Deser, 2016; Sear, Kelly, Jones, & Goodess, 1987) using the eVolv2k volcanic forcing data set (Sigl et al., 2015; Toohey & Sigl, 2017). The reconstructed aerosol optical depth (AOD) can be used as a measure of the size of a volcanic event. In our analysis we include the 13 eruptions over the last millennium with an AOD larger than 0.15. We choose the 14-year intervals spanning from 5 years prior to 9 years after each event. The linear trend is removed from the reconstructed ENSO index over this interval and anomalies are calculated relative to the mean of the years 5 to 1 before the eruption (Dätwyler et al., 2018). Finally, the common response is assessed by taking the mean of these ENSO reconstruction sections aligned across the 13 eruptions. A significance threshold is estimated by applying the same procedure (detrending and centring) to all 14-year long time series around years with no volcanic event. From these, the 90% confidence interval is calculated.

We also analyse the state of ENSO in our new and existing reconstructions in the years before, during and after volcanic eruptions. For this, we transform the reconstructions to anomalies with respect to

a 1961-1990 climatological reference period and check whether the state of ENSO was positive or negative for each year in the time window from -5 to 9 years after an eruption.

3 Results

3.1 ENSO index reconstructions

Performing a PCA over the reference period 1930-1990 using all 81 significantly correlating proxy records over this period yields a PC1 which correlates at r = 0.92 with the target ENSO index, i.e. explaining about 85% of ENSO variance. Removing linear trends over the reference period from the proxy records and target ENSO index prior to the analysis yields an identical result (r = 0.92). This good agreement holds true in the presence of strong large-scale forcing during years after volcanic eruptions (Figures S6-S8), indicating that volcanic forcing peaks do not weaken the ENSO signal in PC1 of the proxy matrix. Calculating the PCs using the proxy records of the five temporal subsets (Section 2.2) yields a correlation between PC1 and the target ENSO index of 0.90 (detrended, 0.90), 0.86 (0.87), 0.83 (0.84), 0.72 (0.72) and 0.67 (0.68) for the 1854, 1800, 1600, 1400 and 1000 subsets, respectively. All correlations are highly significant ($p << 0.01$) and they remain significant if another overlap window is chosen (SM Table S2).

Having demonstrated good relationships between our proxy PC1 and ENSO, we below display the correlation results from our reconstructions obtained using the three different methods and five subsets (Table 1).

Although we do not perform a calibration of the proxy data with the target, we calculate validation statistics over 1901-1929, a period independent from the 1930-1990 window used to select the proxies. We find correlations above r = 0.5 with the target index for all reconstructions except the

Overlap Period PC1 1000 and the *Full Period PC1 1400*. All RE and CE are positive, with the exception of *Overlap Period PC1 1600, 1400 and 1000* and the *Full Period PC1 1400*. The results are shown in Table S3.

To quantify the agreement among the reconstructions we use Pearson's product-moment correlation coefficient. The agreement among the *Running PC1* reconstructions using the five different subsets is between r = 0.97 and 0.43 over 1854-1990 and highly significant ($p << 0.01$) over most of the instrumental period (Figure 2). The agreement remains high back to around 1650, with the exception of the late 19th century (SM Figure S17).

A comparison of our main *Running PC1* with the other two ENSO reconstructions (*Overlap Period PC1* in blue and *Full Period PC1* in green) is shown in Figure 3.

For assessing the periods of simultaneous low agreement across ENSO reconstructions, we only consider periods after 1600, since we have reduced agreement among our reconstructions before 1600 due to the low number of proxy records contributing to the reconstruction (top half, Figure 4). In addition, low verification statistics (particularly in the 1400 subsets) indicate limited reconstruction skill prior to 1600 (see Table S4).

In general we see good agreement in the running correlations between our three different reconstruction methods after 1580, especially in the 17th century and from 1825 onwards, including the whole instrumental period (Figure 4). The earliest period 1000-1400, where only 8 proxy records contributed to the reconstructions shows a diverse picture: a good matching early half (1000-1200 and a late half where there is reduced consensus among the reconstructions (1200-1400). After 1400 there are some time periods where the correlation between our reconstructions breaks down (e.g. during the second half of the 15th century, centred around 1475, and several times for short periods

during the 18th century and at the start of the 19th century until 1825). However, the agreement remains nearly always positive, except for some short periods (e.g., before 1500 or shortly after 1800). These observations are best seen in Figure 4 with the 11-year filter, since some of these features get masked in Figure 3 due to the longer 31-year filter.

3.2 Comparison with existing ENSO reconstructions

Differences in existing ENSO reconstructions (Figure 4) can be seen particularly over the pre-instrumental period. Back to around 1870, the agreement is good (r = 0.66 on average over 1870-2000) and then drops rapidly to an average of r = 0.39 over the period 1806-1869. Nonetheless, there are several other periods (around 1800, 1600, 1460, 1360 and 1310) of high agreement.

Analysing the temporal evolution of simultaneous consistency in our final three reconstructions and the existing reconstructions yields five phases of simultaneous low agreement, where the averaged running correlations are below the first quartile (correlations centred at 1700-1703, 1710-1713, 1730-1738, 1760-1764 and 1773-1786; Figure 4, green vertical lines). The correlations between our main (*Running PC1*) and the existing reconstructions also fall below 0 during four of these five phases (black line in Figure 4).

The average loadings obtained by the running PCA over the five phases of particularly poor reconstruction agreement are shown in Figure 5 (a-e). Negative (i.e. reversed) loadings prevail in the west Pacific/Australasian region during all these periods of low agreement between the reconstructions. That is, the dominant shared pattern of loadings on PC1 over these periods, is not consistent with the observed ENSO-response during the instrumental period. This indicates a change in teleconnection patterns to the western Pacific region during these intervals, all falling within the 18th century.

Loadings for a period of low and high agreement among our new reconstructions, respectively are shown in the SM (Figures S15 and S16).

3.3 Response to volcanic forcing

Superposed epoch analysis of the 13 largest eruptions during the last millennium, all of which are stronger than that of Mt. Pinatubo, yields significant negative NINO3.4 anomalies in our *Running PC1* reconstruction at years three, four and five after eruption time (Figure 6). The strongest negative response occurs four years after the event. The short-term response (year 1) is highly inconsistent, with some eruptions followed by a strong El Niño-like response and others with an apparent La Niña signal.

Figure 7 shows the agreement of the state of ENSO in our new and the existing reconstructions from 5 years before to 9 years after large volcanic eruptions. Our three reconstructions agree on the state of ENSO during the 1109, 1257, 1345, 1695 and 1784 eruptions (bold numbers on the y-axis in Figure 7 and dark-coloured boxes at year 0). For the eruption in 1345 and all following events, with the exception of 1815, at least two thirds of existing reconstructions agree on the state of ENSO at eruption time. However, only two eruptions remain for which the new and existing records show a consistent sign of the state of ENSO during the eruption: 1695 and 1784 (both El Niño phase), as indicated by bold green numbers in Figure 7.

Figure 7 also confirms the negative NINO3.4 anomalies during years 3 to 5 for most eruptions (grey shading). Both the new and existing reconstructions largely agree on negative anomalies, with the exception of 1109 (year 5), 1345 (year 4), 1458 (years 3 and 4) and 1641 (years 4 and 5), 1695 and 1809 (year 5) for the existing reconstructions.

4 Discussion

4.1 New reconstructions

Performing PCA with our five different sets of proxy records yields significant correlations with the target ENSO index over the reference period 1930-1990, for all subsets. Correlations are particularly high for the three most recent subsets. Conditional on this reference period information, these results confirm our initial assumption that the first principal component is a good representation of ENSO back to 1600, and is still reasonable for the 1400 and 1000 subsets. In this respect, despite not performing a formal calibration, our reconstructions perform very well, with equally high or even higher r and r^2 values than reported in the literature for existing reconstruction (see SM Table S3 and S5). The validation statistics (Table S4) for our new reconstructions also demonstrate comparable performance with existing reconstructions. Especially for our most replicated subset (1854 subset) all skill measures (r^2, CE, RE) outperform those reported in previous studies (SM Tables S3, S4 and S5), except for the COA reconstruction in Wilson et al. (2010), which scores an equally high calibration r^2 value for their most replicated nest.

Validation statistics and agreement between our three new reconstructions weaken prior to 1600. The main reason for the lower validation statistics is the low number (n = 18) of proxy records prior to 1600 (n = 8 prior to 1400). With such a limited amount of input data, the PC1 approach is more likely to be biased by individual records and may become less skilful than a classical calibration approach. The low number of records also leads to non-climatic fluctuations in the running loadings (SM Section 9, Figures S18-S22) pointing towards a limitation of our method when the number of input datasets is low.

Our reconstructions since 1600 are generally robust against the choice of method and yield high performance statistics back to 1600. Due to this good agreement among our three different reconstructions, we hypothesise that ENSO teleconnections are likely to have been stationary over most of the last 400 years, given the large network of proxy records we use. From 1600 on, with 32 proxy records, the network appears generally large enough to compensate for local to regional effects, changes in teleconnections and/or effects of changing amount of noise in the proxy records over time, even if no records from the centre of action of ENSO (the central and eastern tropical Pacific) are available (e.g., Batehup et al., 2015). Hence we consider the value of around 30 records to be a good estimate of the minimum number of (teleconnected) records to obtain reliable ENSO reconstructions.

4.2 Comparison with existing reconstructions

The existing reconstructions show reduced agreement prior to the instrumental period. The differences stem from various possible sources: a) the use of different reconstruction targets and seasons, b) the use of different proxy archives and records, c) local climate or biologically caused noise, and d) uncertainties in the proxy records or changing teleconnections (Batehup et al., 2015; Gergis & Fowler, 2009; McGregor et al., 2010; van Oldenborgh & Burgers, 2005). We identify five phases (1700-1703, 1710-1713, 1730-1738, 1760-1764 and 1773-1786) of simultaneous low agreement across our new and the existing reconstructions. During all these periods we find a consistent teleconnection pattern that is different to the teleconnections of ENSO in the instrumental period. These differences are mainly in the west Pacific/Australasian domain where the sign of the common climate response is opposite to expected from ENSO today, suggesting that there was a change in ENSO teleconnections around these intervals (Figure 5). Possible causes for

this changed response pattern include changes in ENSO flavours (Johnson, 2013), changes in the interplay and relative strength of ENSO with other forms of climate variability such as the Indian Ocean Dipole or the Asian-Australasian monsoon system (Ham, Choi, & Kug, 2017; Luo et al., 2010), or shifts in the position or strength of the South Pacific Convergence Zone (SPCZ, Juillet-Leclerc et al., 2006; Linsley et al., 2006; McGregor, Timmermann, Schneider, Stuecker, & England, 2012; Saint-Lu, Braconnot, Leloup, Lengaigne, & Marti, 2015).

4.3 Response to volcanic forcing

Our assessment of new and existing ENSO reconstructions provides a basis for re-evaluating the connection of ENSO variability with volcanic eruptions during the last millennium. Using a SEA, we show that 3 to 5 years after major volcanic events the ENSO index responds with a significant tendency towards more La Niña-like conditions. This is consistent with several previous studies. Wahl et al. (2014) evaluated late boreal winter temperature responses to strong volcanic eruptions in western North America. They found a La Niña-like response in post-event years 3-5, with year 3 having the most spatially significant and coherent response. Furthermore, D'Arrigo et al. (2009), who differentiate between low- and high latitude eruptions, also found a cooling signature persisting for several years after the event. Liu et al. (2018) distinguish between NH, tropical and SH eruptions. They showed that NH and tropical eruptions can provoke El Niño-like responses within 2 years after the event, whereas SH eruptions are more likely to cause La Niña-like responses delayed by 3 years. In contrast to our results, which are not clear about post-eruption year 1, Emile-Geay et al. (2008) demonstrated an increased likelihood of El Niño events in the year following volcanic eruptions larger than that of Mt. Pinatubo, using model results. Based on two paleoclimate reconstructions Adams et al. (2003) also showed a multi-year El Niño-like response of ENSO to explosive tropical

volcanic eruptions, along with significant La Niña-like responses in years 4-6. This shift towards negative SSTs was also found by Wilson et al. (2010) at years 4 and 7. Using the CESM (Community Earth System Model), Sun et al. (2018) also found a transition from El Niño-like to a significant La Niña-like state after large tropical eruptions; however, the significant La Niña-like state already occurred two years after the eruptions. The apparent discrepancies in the literature on the response of ENSO to volcanic forcing, illustrate that there is no consensus yet. Proxy-based ENSO reconstructions provide little agreement on a common ENSO response to volcanic eruptions, and climate models offer various explanations for the underlying mechanisms (Liu et al., 2018; McGregor & Timmermann, 2010; Ohba et al., 2013; Stevenson et al., 2017). Possible factors that may contribute to the heterogeneous picture in the literature on the relationship between volcanic forcing and ENSO include the fact that the (often unknown) season and prevailing ocean-atmospheric conditions, in combination with the geographic location of the eruption, have impacts on the way that volcanic aerosols get distributed and the climatic effects they have (Hegerl, Crowley, Hyde, & Frame, 2006; Kravitz & Robock, 2011; Toohey, Krüger, Niemeier, & Timmreck, 2011, cf. Wahl et al., 2014).

Knowledge of the state of ENSO at the time of volcanic events may be crucial to help explaining over- or under-estimation of climatic responses to volcanic eruptions in climate models. Lehner et al. (2016) showed that the state of ENSO strongly influences the global temperature response to volcanic eruptions, since all large eruptions they considered since 1951 happened to fall together with El Niño events (cf. Wahl et al., 2014 for energy-balance consideration of how the initial state of ENSO can modulate the effect of volcanic forcing on the climate system). Our analysis compiles the paleoclimate information in new and existing ENSO reconstructions and reveals that, with high likelihood, there were El Niño-like conditions prevailing during the 1695 and 1784 eruptions. For

these years we suggest that robust analyses of the influence of ENSO state on global and regional temperature and hydroclimate response are possible, as is data-model comparison. For all other events, the state of ENSO during the eruptions remains uncertain.

5 Conclusions and Outlook

Our new ENSO reconstructions are based on a large, updated collection of proxy records and use the simple but efficient PCA method. They agree highly with the target ENSO index over the instrumental period and show high reconstruction skill during the period with sufficient proxy data coverage (post-1600). We have shown that the analysis with sliding time windows allows us to dynamically capture variations over time that are potentially caused by changes in teleconnections. We are able to provide particularly robust estimates of ENSO from 1580 to the end of the 17th century and from 1825 to present. Further work is needed to identify the causes of reduced coherence in the various ENSO reconstructions in the intervals identified herein (particularly during the 18th century) and during volcanic eruptions. This may be achieved by pseudoproxy experiments (Smerdon, 2012), which allow for examining dynamical changes in the model world that can lead to changing teleconnection patterns. Pseudoproxy experiments can additionally be used to test the influence of proxy noise and reconstruction method on reconstructed teleconnection stability and reconstruction robustness (Neukom, Schurer, Steiger, & Hegerl, 2018). Finally, pseudoproxy experiments can open up the possibility to improve estimates of minimum proxy numbers and spatial distribution for robust and stationary ENSO reconstructions.

Acknowledgements

This work partly resulted from contributions to the Past Global Changes (PAGES) 2k initiative. Members of the PAGES2k consortium are thanked for providing public access to proxy data and metadata. This study was supported by the Swiss National Science Foundation (SNF) Ambizione grant PZ00P2_154802. RN and CD designed the study; CD led the writing, conducted the data analysis and made the figures (except Figure 7 made by RN). All authors jointly discussed and contributed to the writing. The authors thank two anonymous reviewers for their suggestions and comments on this study.

Conflict of interest

The authors declare that they have no conflicts of interest.

Data availability

Our proxy data and reconstructions results are available at the NOAA paleoclimatology database ([LINK]).

Supporting information

This article contains supplementary material which is available online.

Data Citations

1. PAGES 2k Consortium. (2017). *figshare.* https://doi.org/10.6084/m9.figshare.c.3285353

2. Neukom, R., Gergis, J., Karoly, D. J., Wanner, H., Curran, M., Elbert, J.,. . . Frank, D. (2014). *World Data Service for Paleoclimatology.* https://www.ncdc.noaa.gov/paleo/study/16196

3. Stenni, B., Curran, M. A. J., Abram, N. J., Orsi, A., Goursaud, S., Masson-Delmotte, V,. . . Frezotti, M. (2017). *World Data Service for Paleoclimatology.* https://www.ncdc.noaa.gov/paleo/study/22589

4. Emile-Geay, J., Cobb, K. M., Mann, M. E., & Wittenberg, A. T. (2013). *World Data Service for Paleoclimatology.* https://www.ncdc.noaa.gov/paleo/study/13684

5. Henke, L. M. K., Lambert, F. H., & Charman, D. J. (2017). *figshare.* https://doi.org/10.6084/m9.figshare.4787575

References

Adams, J. B., Mann, M. E., & Ammann, C. M. (2003). Proxy evidence for an El Niño-like response to volcanic forcing. *Nature*, *426*, 274-278. https://doi.org/10.1038/nature02101

Barnston, A. G., Chelliah, M., & Goldenberg, S. B. (1997). Documentation of a highly ENSO-related sst region in the equatorial pacific: Research note. *Atmosphere-Ocean*, *35*(3), 367–383. https://doi.org/10.1080/07055900.1997.9649597

Batehup, R., McGregor, S., & Gallant, A. J. E. (2015). The influence of non-stationary teleconnections on palaeoclimate reconstructions of ENSO variance using a pseudoproxy framework. *Climate of the Past*, *11*(12), 1733–1749. https://doi.org/10.5194/cp-11-1733-2015

Becker, R. A., Chambers, J. M., & Wilks, A. R. (1988). *The New S Language, A Programming Environment for Data Analysis and Graphics.*

Bradley, R. S., Diaz, H. F., Kiladis, G. N., & Eischeid, J. K. (1987). ENSO signal in continental temperature and precipitation records. *Nature*, *327*(6122), 497–501. https://doi.org/10.1038/327497a0

Braganza, K., Gergis, J. L., Power, S. B., Risbey, J. S., & Fowler, A. M. (2009). A multiproxy index of the El Niño–Southern Oscillation, A.D. 1525–1982. *Journal of Geophysical Research: Atmospheres*, *114*(D5). https://doi.org/10.1029/2008JD010896

Brönnimann, S. (2007). Impact of El Niño–Southern Oscillation on European climate. *Reviews of Geophysics*, *45*(3). https://doi.org/10.1029/2006RG000199

Cook, E. R., Briffa, K. R., & Jones, P. D. (1994). Spatial regression methods in dendroclimatology: A review and comparison of two techniques. *International Journal of Climatology*, *14*(4), 379–402. https://doi.org/10.1002/joc.3370140404

Cook, E. R., D'Arrigo, R. D., & Anchukaitis, K. J. (2008, April). *ENSO reconstructions from long tree-ring chronologies: Unifying the differences?* Talk presented at a special workshop on "Reconciling ENSO Chronologies for the Past 500 Years", Moorea, French Polynesia.

D'Arrigo, R., Wilson, R., & Tudhope, A. (2009). The impact of volcanic forcing on tropical temperatures during the past four centuries. *Nature Geoscience*, *2*, 51 -56. https://doi.org/10.1038/ngeo393

D'Arrigo, R., Cook, E. R., Wilson, R. J., Allan, R., & Mann, M. E. (2005). On the variability of ENSO over the past six centuries. *Geophysical Research Letters*, *32*(3). https://doi.org/10.1029/2004GL022055

Dätwyler, C., Neukom, R., Abram, N. J., Gallant, A. J. E., Grosjean, M., Jacques-Coper, M., . . . Villalba, R. (2018). Teleconnection stationarity, variability and trends of the Southern Annular Mode (SAM) during the last millennium. *Climate Dynamics*, *51*(5), 2321–2339. https://doi.org/10.1007/s00382-017-4015-0

Emile-Geay, J., Cobb, K. M., Mann, M. E., & Wittenberg, A. T. (2013). Estimating Central Equatorial Pacific SST Variability over the Past Millennium. Part II: Reconstructions and Implications. *Journal of Climate*, *26*(7), 2329–2352. https://doi.org/10.1175/JCLI-D-11-00511.1

Emile-Geay, J., Seager, R., Cane, M. A., Cook, E. R., & Haug, G. H. (2008). Volcanoes and ENSO over the Past Millennium. *Journal of Climate*, *21*(13), 3134–3148. https://doi.org/10.1175/2007JCLI1884.1

Gergis, J. L., & Fowler, A. M. (2009). A history of ENSO events since A.D. 1525: Implications for future climate change. *Climatic Change*, *92*(3), 343–387. https://doi.org/10.1007/s10584-008-9476-z

Ham, Y.-G., Choi, J.-Y., & Kug, J.-S. (2017). The weakening of the ENSO–Indian Ocean Dipole (IOD) coupling strength in recent decades. *Climate Dynamics*, *49*(1), 249–261. https://doi.org/10.1007/s00382-016-3339-5

Haurwitz, M. W., & Brier, G. W. (1981). A Critique of the Superposed Epoch Analysis Method: Its Application to Solar–Weather Relations. *Mon. Wea. Rev.*, *109*(10), 2074–2079. https://doi.org/10.1175/1520-0493(1981)109<2074:ACOTSE>2.0.CO;2

Hegerl, G. C., Crowley, T. J., Hyde, W. T., & Frame, D. J. (2006). Climate sensitivity constrained by temperature reconstructions over the past seven centuries. *Nature*, *440*(7087), 1029–1032. https://doi.org/10.1038/nature04679

Huang, B., Thorne, P. W., Banzon, V. F., Boyer, T., Chepurin, G., Lawrimore, J. H., . . . Zhang, H.-M. (2017). Extended Reconstructed Sea Surface Temperature, Version 5 (ERSSTv5): Upgrades, Validations, and Intercomparisons. *Journal of Climate*, *30*(20), 8179–8205. https://doi.org/10.1175/JCLI-D-16-0836.1

Iles, C. E., & Hegerl, G. C. (2015). Systematic change in global patterns of streamflow following volcanic eruptions. *Nature Geoscience*, *8*, 838 - 842. https://doi.org/10.1038/ngeo2545

Johnson, N. C. (2013). How Many ENSO Flavors Can We Distinguish? *J. Climate*, *26*(13), 4816–4827. https://doi.org/10.1175/JCLI-D-12-00649.1

Juillet-Leclerc, A., Thiria, S., Naveau, P., Delcroix, T., Le Bec, N., Blamart, D., & Corrège, T. (2006). SPCZ migration and ENSO events during the 20th century as revealed by climate proxies from a Fiji coral. *Geophysical Research Letters*, *33*(17). https://doi.org/10.1029/2006GL025950

Kravitz, B., & Robock, A. (2011). Climate effects of high-latitude volcanic eruptions: Role of the time of year. *Journal of Geophysical Research*, *116*(D1). https://doi.org/10.1029/2010JD014448

Lehner, F., Schurer, A. P., Hegerl, G. C., Deser, C., & Frölicher, T. L. (2016). The importance of ENSO phase during volcanic eruptions for detection and attribution. *Geophysical Research Letters*, *43*(6), 2851–2858. https://doi.org/10.1002/2016GL067935

Li, J., Xie, S.-P., Cook, E. R., Huang, G., D'Arrigo, R., Liu, F., . . . Zheng, X.-T. (2011). Interdecadal modulation of El Niño amplitude during the past millennium. *Nature Climate Change*, *1*, 114. https://doi.org/10.1038/nclimate1086

Li, J., Xie, S.-P., Cook, E. R., Morales, M. S., Christie, D. A., Johnson, N. C., . . . Fang, K. (2013). El Niño modulations over the past seven centuries. *Nature Climate Change*, *3*, 822 - 826. https://doi.org/10.1038/nclimate1936

Linsley, B. K., Kaplan, A., Gouriou, Y., Salinger, J., deMenocal, P. B., Wellington, G. M., & Howe, S. S. (2006). Tracking the extent of the South Pacific Convergence Zone since the early 1600s. *Geochemistry, Geophysics, Geosystems*, *7*(5). https://doi.org/10.1029/2005GC001115

Liu, F., Li, J., Wang, B., Liu, J., Li, T., Huang, G., & Wang, Z. (2018). Divergent El Niño responses to volcanic eruptions at different latitudes over the past millennium. *Climate Dynamics*, *50*(9), 3799–3812. https://doi.org/10.1007/s00382-017-3846-z

Luo, J.-J., Zhang, R., Behera, S. K., Masumoto, Y., Jin, F.-F., Lukas, R., & Yamagata, T. (2010). Interaction between El Niño and Extreme Indian Ocean Dipole. *J. Climate*, *23*(3), 726–742. https://doi.org/10.1175/2009JCLI3104.1

Mann, M. E., Zhang, Z., Rutherford, S., Bradley, R. S., Hughes, M. K., Shindell, D., . . . Ni, F. (2009). Global Signatures and Dynamical Origins of the Little Ice Age and Medieval Climate Anomaly. *Science (New York, N.Y.)*, *326*(5957), 1256–1260. https://doi.org/10.1126/science.1177303

Mardia, K. V., Kent, J. T., & Bibby, J. M. (1979). *Multivariate analysis*. *Probability and mathematical statistics*. London, New York: Academic Press.

McGraw, M. C., Barnes, E. A., & Deser, C. (2016). Reconciling the observed and modeled Southern Hemisphere circulation response to volcanic eruptions. *Geophysical Research Letters*, *43*(13), 7259–7266. https://doi.org/10.1002/2016GL069835

McGregor, S., Timmermann, A., England, M. H., Elison Timm, O., & Wittenberg, A. T. (2013). Inferred changes in El Niño–Southern Oscillation variance over the past six centuries. *Climate of the Past*, *9*(5), 2269–2284. https://doi.org/10.5194/cp-9-2269-2013

McGregor, S., Timmermann, A., & Timm, O. (2010). A unified proxy for ENSO and PDO variability since 1650. *Climate of the Past*, *6*(1), 1–17. https://doi.org/10.5194/cp-6-1-2010

McGregor, S., & Timmermann, A. (2010). The Effect of Explosive Tropical Volcanism on ENSO. *Journal of Climate*, *24*(8), 2178–2191. https://doi.org/10.1175/2010JCLI3990.1

McGregor, S., Timmermann, A., Schneider, N., Stuecker, M. F., & England, M. H. (2012). The Effect of the South Pacific Convergence Zone on the Termination of El Niño Events and the Meridional Asymmetry of ENSO. *J. Climate*, *25*(16), 5566–5586. https://doi.org/10.1175/JCLI-D-11-00332.1

McPhaden, M. J., Zebiak, S. E., & Glantz, M. H. (2006). ENSO as an Integrating Concept in Earth Science. *Science*, *314*(5806), 1740–1745. https://doi.org/10.1126/science.1132588

Neelin, J. D., Battisti, D. S., Hirst, A. C., Jin, F.-F., Wakata, Y., Yamagata, T., & Zebiak, S. E. (1998). ENSO theory. *Journal of Geophysical Research*, *103*(C7), 14261–14290. https://doi.org/10.1029/97JC03424

Neukom, R., Gergis, J., Karoly, D. J., Wanner, H., Curran, M., Elbert, J., . . . Frank, D. (2014). Inter-hemispheric temperature variability over the past millennium. *Nature Climate Change*, *4*(5), 362–367. https://doi.org/10.1038/nclimate2174

Neukom, R., Schurer, A. P., Steiger, N. J., & Hegerl, G. C. (2018). Possible causes of data model discrepancy in the temperature history of the last Millennium. *Scientific Reports*, *8*(1), 7572. https://doi.org/10.1038/s41598-018-25862-2

Ohba, M., Shiogama, H., Yokohata, T., & Watanabe, M. (2013). Impact of Strong Tropical Volcanic Eruptions on ENSO Simulated in a Coupled GCM. *Journal of Climate*, *26*(14), 5169–5182. https://doi.org/10.1175/JCLI-D-12-00471.1

PAGES 2k-PMIP3 group. (2015). Continental-scale temperature variability in PMIP3 simulations and PAGES 2k regional temperature reconstructions over the past millennium. *Climate of the Past*, *11*(12), 1673–1699. https://doi.org/10.5194/cp-11-1673-2015

Raible, C. C., Brönnimann, S., Auchmann, R., Brohan, P., Frölicher, T. L., Graf, H.-F., . . . Wegmann, M. (2016). Tambora 1815 as a test case for high impact volcanic eruptions: Earth system effects. *Wiley Interdisciplinary Reviews: Climate Change*, *7*(4), 569–589. https://doi.org/10.1002/wcc.407

Saint-Lu, M., Braconnot, P., Leloup, J., Lengaigne, M., & Marti, O. (2015). Changes in the ENSO/SPCZ relationship from past to future climates. *Earth and Planetary Science Letters*, *412*, 18–24. https://doi.org/10.1016/j.epsl.2014.12.033

Santer, B. D., Wigley, T. M. L., Boyle, J. S., Gaffen, D. J., Hnilo, J. J., Nychka, D., . . . Taylor, K. E. (2000). Statistical significance of trends and trend differences in layer-average atmospheric temperature time series. *Journal of Geophysical Research*, *105*(D6), 7337–7356. https://doi.org/10.1029/1999JD901105

Sear, C. B., Kelly, P. M., Jones, P. D., & Goodess, C. M. (1987). Global surface-temperature responses to major volcanic eruptions. *Nature*, *330*(6146), 365–367. https://doi.org/10.1038/330365a0

Sigl, M., Winstrup, M., McConnell, J. R., Welten, K. C., Plunkett, G., Ludlow, F., . . . Woodruff, T. E. (2015). Timing and climate forcing of volcanic eruptions for the past 2,500 years. *Nature*, *523*(7562), 543–549. https://doi.org/10.1038/nature14565

Smerdon, J. E. (2012). Climate models as a test bed for climate reconstruction methods: Pseudoproxy experiments. *Wiley Interdisciplinary Reviews: Climate Change*, *3*(1), 63–77. https://doi.org/10.1002/wcc.149

Stahle, D. W., Cleaveland, M. K., Therrell, M. D., Gay, D. A., D'Arrigo, R. D., Krusic, P. J., . . . Thompson, L. G. (1998). Experimental Dendroclimatic Reconstruction of the Southern Oscillation. *Bulletin of the American Meteorological Society*, *79*(10), 2137–2152. https://doi.org/10.1175/1520-0477(1998)079<2137:EDROTS>2.0.CO;2

Standard Error of Prediction and Confidence Limits. (2018). Retrieved from https://www.jmp.com/support/help/14/standard-error-of-prediction-and-confidence-limi.shtml

Stevenson, S., Fasullo, J. T., Otto-Bliesner, B. L., Tomas, R. A., & Gao, C. (2017). Role of eruption season in reconciling model and proxy responses to tropical volcanism. *Proceedings of the National Academy of Sciences*, *114*(8), 1822–1826. https://doi.org/10.1073/pnas.1612505114

Su, H., Neelin, J. D., & Meyerson, J. E. (2005). Mechanisms for Lagged Atmospheric Response to ENSO SST Forcing. *Journal of Climate*, *18*(20), 4195–4215. https://doi.org/10.1175/JCLI3514.1

Sun, W., Liu, J., Wang, B., Chen, D., Liu, F., Wang, Z., . . . Chen, M. (2018). A “La Niña-like” state occurring in the second year after large tropical volcanic eruptions during the past 1500 years. *Climate Dynamics.* Advance online publication. https://doi.org/10.1007/s00382-018-4163-x

Tierney, J. E., Abram, N. J., Anchukaitis, K. J., Evans, M. N., Giry, C., Kilbourne, K. H., . . . Zinke, J. (2015). Tropical sea surface temperatures for the past four centuries reconstructed from coral archives. *Paleoceanography*, *30*(3), 226–252. https://doi.org/10.1002/2014PA002717

Toohey, M., Krüger, K., Niemeier, U., & Timmreck, C. (2011). The influence of eruption season on the global aerosol evolution and radiative impact of tropical volcanic eruptions. *Atmospheric Chemistry and Physics*, *11*(23), 12351–12367. https://doi.org/10.5194/acp-11-12351-2011

Toohey, M., & Sigl, M. (2017). Volcanic stratospheric sulfur injections and aerosol optical depth from 500 BCE to 1900 CE. *Earth Syst. Sci. Data*, *9*(2), 809–831. https://doi.org/10.5194/essd-9-809-2017

Van Oldenborgh, G. J., & Burgers, G. (2005). Searching for decadal variations in ENSO precipitation teleconnections. *Geophysical Research Letters*, *32*(15). https://doi.org/10.1029/2005GL023110

Venables, W. N., & Ripley, B. D. (2002). *Modern Applied Statistics with S* (4th ed.). New York: Springer-Verlag.

Wahl, E. R., Diaz, H. F., Smerdon, J. E., & Ammann, C. M. (2014). Late winter temperature response to large tropical volcanic eruptions in temperate western North America: Relationship to ENSO phases. *Global and Planetary Change*, *122*, 238–250. https://doi.org/10.1016/j.gloplacha.2014.08.005

Wilson, R., Cook, E., D'Arrigo, R., Riedwyl, N., Evans, M. N., Tudhope, A., & Allan, R. (2010). Reconstructing ENSO: The influence of method, proxy data, climate forcing and teleconnections. *Journal of Quaternary Science*, *25*(1), 62–78. https://doi.org/10.1002/jqs.1297

Yan, H., Sun, L., Wang, Y., Huang, W., Qiu, S., & Yang, C. (2011). A record of the Southern Oscillation Index for the past 2,000 years from precipitation proxies. *Nature Geoscience*, *4*, 611 - 614. https://doi.org/10.1038/ngeo1231

Yeh, S.-W., Cai, W., Min, S.-K., McPhaden, M. J., Dommenget, D., Dewitte, B., . . . Kug, J.-S. (2018). ENSO Atmospheric Teleconnections and Their Response to Greenhouse Gas Forcing. *Reviews of Geophysics*, *56*(1), 185–206. https://doi.org/10.1002/2017RG000568

ENSO variability, teleconnection changes and responses to large volcanic eruptions since AD 1000

Christoph Dätwyler*, Nerilie J. Abram, Martin Grosjean, Eugene R. Wahl and Raphael Neukom

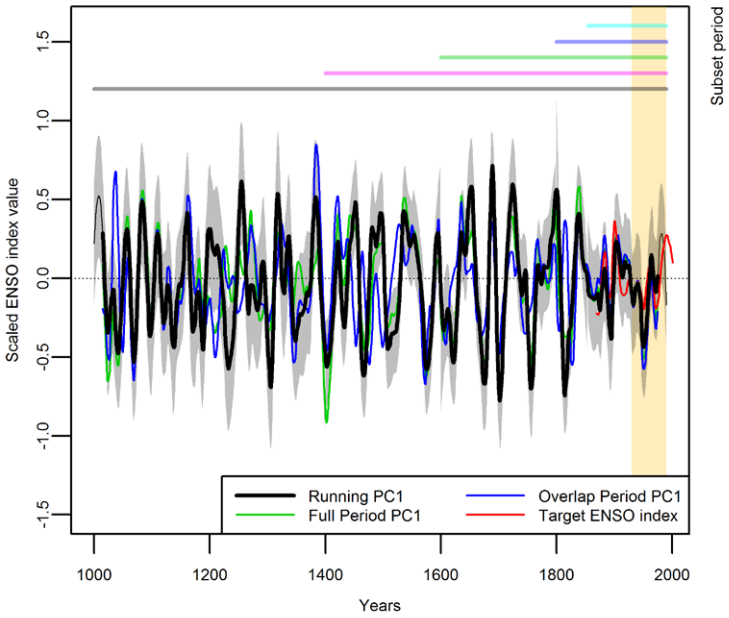

This study provides new ENSO reconstructions based on a large, updated collection of proxy records. We identify the periods from 1580 to the end of the 17th century and from 1825 to present as most robust to quantify ENSO within the last millennium, and reveal disagreement among various ENSO reconstructions during five periods within 1700-1786, possibly related to teleconnection changes in the west Pacific domain. We find a significant response of ENSO towards more La Niña-like conditions 3-5 years after major volcanic events.

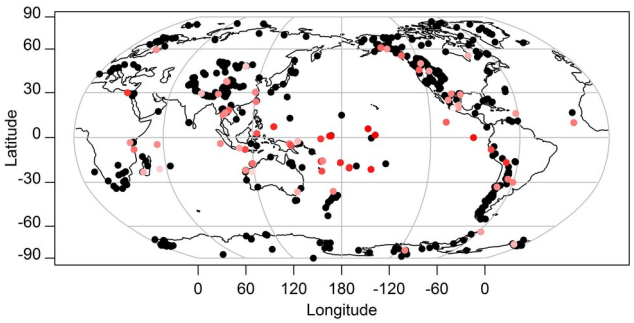

JOC_5983_Figure_1.jpg

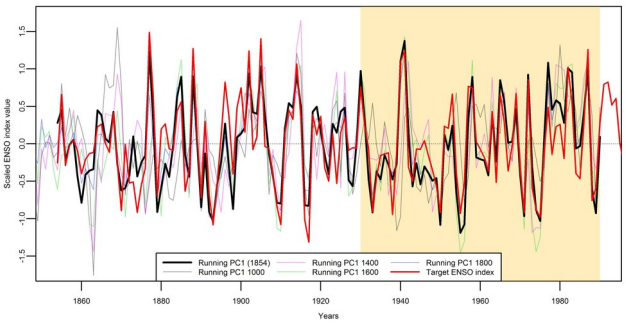

JOC_5983_Figure_2.jpg

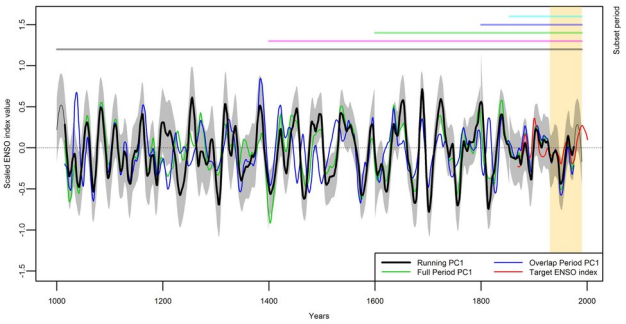

JOC_5983_Figure_3.jpg

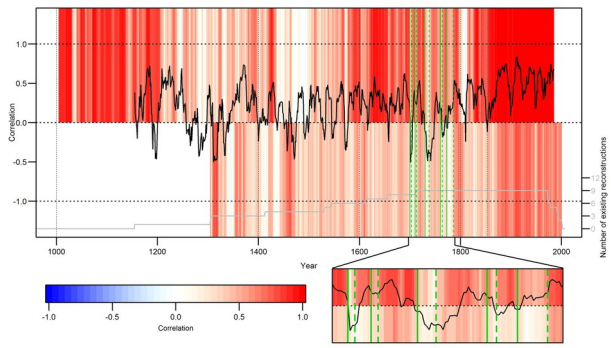

JOC_5983_Figure_4.jpg

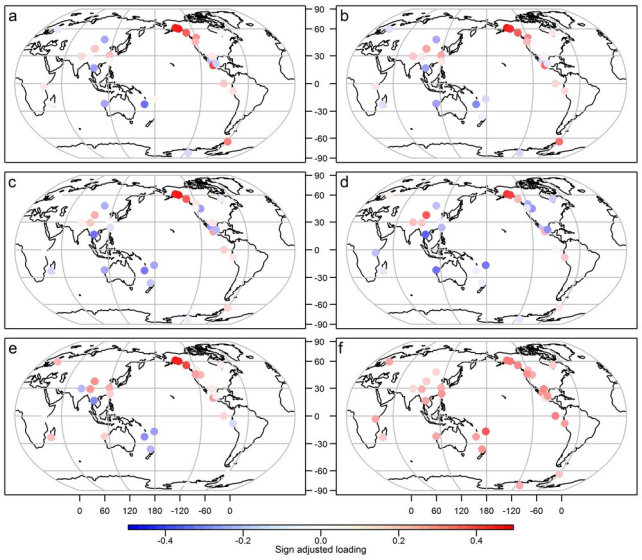

JOC_5983_Figure_5.jpg

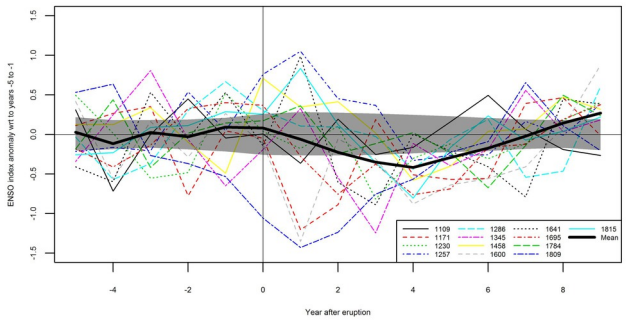

JOC_5983_Figure_6.jpg

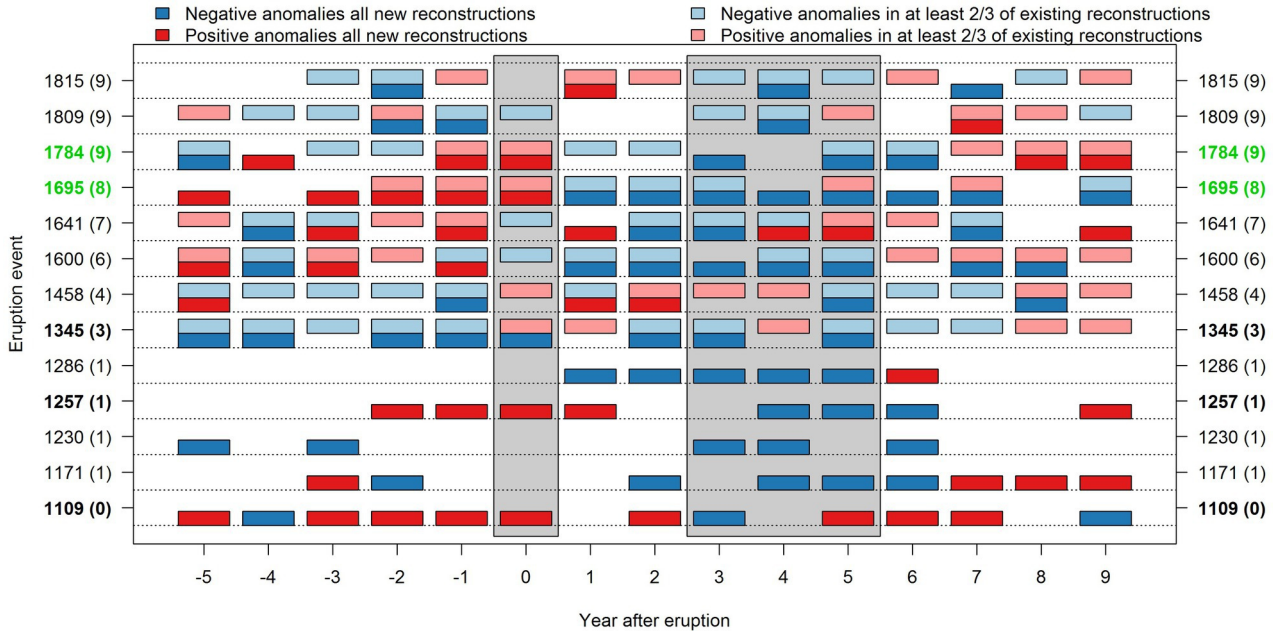

JOC_5983_Figure_7.jpg

Table 1 *Correlation (r) between the target instrumental ENSO index (with 80-year trends removed) and the reconstructions over the reference period 1930-1990 for the five subsets and three methods. All correlations are significant ($p < 0.05$)*

Reconstruction	r	Reconstruction	r	Reconstruction	r
Running PC1 1854	0.90	Overlap Period PC1 1854	0.90	Full Period PC1 1854	0.91
Running PC1 1800	0.87	Overlap Period PC1 1800	0.86	Full Period PC1 1800	0.86
Running PC1 1600	0.82	Overlap Period PC1 1600	0.78	Full Period PC1 1600	0.64
Running PC1 1400	0.61	Overlap Period PC1 1400	0.48	Full Period PC1 1400	0.64
Running PC1 1000	0.33	Overlap Period PC1 1000	0.51	Full Period PC1 1000	0.43